Magnetic Resonance Imaging 60 (2019) 93–100

Contents lists available at ScienceDirect

Magnetic Resonance Imaging

journal homepage: www.elsevier.com/locate/mri

Original contribution

Plaque components segmentation in carotid artery on simultaneous non-contrast angiography and intraplaque hemorrhage imaging using machine learning

Qiang Zhang[a], Huiyu Qiao[a], Jiaqi Dou[a], Binbin Sui[b], Xihai Zhao[a], Zhensen Chen[a], Yishi Wang[a,c], Shuo Chen[a], Mingquan Lin[d], Bernard Chiu[d], Chun Yuan[a,e], Rui Li[a,*], Huijun Chen[a,**]

[a] Center for Biomedical Imaging Research, Department of Biomedical Engineering, School of Medicine, Tsinghua University, Beijing, China
[b] Department of Radiology, Beijing TianTan Hospital, Capital Medical University, Beijing Neurosurgical Institute, Beijing, China
[c] Philips Healthcare, Beijing, China
[d] Department of Electronic Engineering, City University of Hong Kong, Hong Kong, China
[e] Vascular Imaging Laboratory, Department of Radiology, University of Washington, Seattle, WA, USA

ARTICLE INFO

Keywords:
SNAP
Carotid atherosclerosis
Plaque components
Segmentation

ABSTRACT

Purpose: This study sought to determine the feasibility of using Simultaneous Non-contrast Angiography and intraPlaque Hemorrhage (SNAP) to detect the lipid-rich/necrotic core (LRNC), and develop a machine learning based algorithm to segment plaque components on SNAP images.

Methods: Sixty-eight patients (age: 58 ± 9 years, 24 males) with carotid artery atherosclerotic plaque were imaged on a 3 T MR scanner with both traditional multi-contrast vessel wall MR sequences (TOF, T1W, and T2W) and 3D SNAP sequence. The manual segmentations of carotid plaque components including LRNC, intraplaque hemorrhage (IPH), calcification (CA) and fibrous tissue (FT) on traditional multi-contrast images were used as reference. By utilizing the intensity and morphological information from SNAP, a machine learning based two steps algorithm was developed to firstly identify LRNC (with or without IPH), CA and FT, and then segmented IPH from LRNC. Ten-fold cross-validation was used to evaluate the performance of proposed method. The overall pixel-wise accuracy, the slice-wise sensitivity & specificity & Youden's index, and the Pearson's correlation coefficient of the component area between the proposed method and the manual segmentation were reported.

Results: In the first step, all tested classifiers (Naive Bayes (NB), Support Vector Machine (SVM), Random Forest (RF), Gradient Boosting Decision Tree (GBDT) and Artificial Neural Network (ANN)) had overall pixel-wise accuracy higher than 0.88. For RF, GBDT and ANN classifiers, the correlation coefficients of areas were all higher than 0.82 ($p < 0.001$) for LRNC and 0.79 for CA ($p < 0.001$), and the Youden's indexes were all higher than 0.79 for LRNC and 0.76 for CA, which were better than that of NB and SVM. In the second step, the overall pixel-wise accuracy was higher than 0.78 for the five classifiers, and RF achieved the highest Youden's index (0.69) with the correlation coefficients as 0.63 ($p < 0.001$).

Conclusions: The RF is the overall best classifier for our proposed method, and the feasibility of using SNAP to identify plaque components, including LRNC, IPH, CA, and FT has been validated. The proposed segmentation method using a single SNAP sequence might be a promising tool for atherosclerotic plaque components assessment.

1. Introduction

Stroke is one of the leading causes of death and disability in the world [1], and is commonly associated with unstable carotid atherosclerotic plaques. The intraplaque hemorrhage can be used to predict recurrent ischemia and stroke [2], large necrotic core is related to

* Correspondence to: R. Li, Center for Biomedical Imaging Research #110, Department of Biomedical Engineering, School of Medicine, Tsinghua University, Beijing, China.
** Correspondence to: H. Chen, Center for Biomedical Imaging Research #109, Department of Biomedical Engineering, School of Medicine, Tsinghua University, Beijing, China.
E-mail addresses: leerui@tsinghua.edu.cn (R. Li), chenhj_cbir@mail.tsinghua.edu.cn (H. Chen).

https://doi.org/10.1016/j.mri.2019.04.001
Received 28 December 2018; Received in revised form 27 February 2019; Accepted 2 April 2019

plaque structural weakness [3], and calcification is related to vulnerability of plaques [4]. The compositional characteristics of atherosclerotic plaque have been demonstrated to be related to clinical events [3,5].

Morphology and composition of atherosclerotic plaques can be characterized and identified on traditional multi-contrast MR images using established criteria [6–8]. Some machine learning based automatic algorithms have been proposed for plaque components segmentation, including the minimum distance classifier algorithm [9,10] and the cluster algorithm [11] based on image intensity. Liu et al. [12] proposed a method that employed the local wall morphological features as well as the image intensity, and successfully improved the segmentation performance.

However, traditional multi-contrast MR images require long scan time, and the possible misregistration among different weightings poses a challenge on the image analysis. Recently, a 3D Simultaneous Non-contrast Angiography and Intraplaque Hemorrhage (SNAP) sequence [13] has been proposed for carotid plaque imaging with large coverage. This sequence consists of an inversion pulse followed by two gradient echo acquisitions: an inversion recovery acquisition (IR), which is highly T1 weighted, and a reference acquisition (REF), which is proton density (PD) weighted. The REF is used to correct the background phase of the IR acquisition in the original SNAP to generate a phase-sensitive reconstruction (CR) image [13], in which intraplaque hemorrhage (IPH) shows hyper-intensity signal and the artery lumen shows negative value. Moreover, angiographic images can be generated by applying minimum intensity projection to the CR images. Recently, a new contrast (SNAP2 [14]), which can be calculated from IR and REF of SNAP, was proposed for calcification detection. Previous studies have demonstrated that SNAP can be used to detect intraplaque hemorrhage [13], artery surface characteristics (including juxtaluminal calcification and ulceration) [15] and calcification [16]. In addition, a recent study [17] has reported that heavily T1 weighted sequence (MPRAGE) can be used to identify LRNC. Since SNAP is also heavily T1 weighted, the SNAP may also be used to identify LRNC. However, plaque components identification in these studies are all done manually by experienced radiologists, which is time consuming and limits the usage of SNAP in clinical practice.

The goal of this study was to develop a segmentation method for plaque components using a single SNAP sequence. In this study, using the manual segmentation which delineated from traditional carotid artery multi-contrast images as reference, both the intensities of multiple contrast SNAP images and the morphological information were extracted as features, and five machine learning classifiers were used for plaque components segmentation.

2. Materials and methods

2.1. Study data

In this retrospective study, a total of 68 patients (age: 58 ± 9 years, 24 males) were included in which all patients underwent recent stroke or transient ischemic attack within 2 weeks and carotid artery atherosclerotic plaque in at least one carotid artery determined by ultrasound (intima-media thickness ≥ 1.5 mm). The exclusion criteria included: (1) patients with evidence of cardiogenic stroke; (2) patients with hemorrhagic stroke; (3) history of radiation therapy in the neck; (4) claustrophobia and (5) contraindication to MRI examination. All the patients were imaged with both traditional multi-contrast and SNAP sequences on a whole body 3.0 Tesla MR scanner (Achieva TX, Philips Healthcare, Best, The Netherlands) with a custom-designed 36-channel neurovascular coil [18] in Tsinghua University. The traditional multi-contrast imaging protocol included three-dimensional time-of-flight (3D-TOF), 2D quadruple inversion-recovery T1-weighted imaging (T1W-QIR) [19] and 2D double inversion-recovery T2-weighted imaging (T2W-DIR) [20]. For the traditional multi-contrast imaging, all the acquisitions were centered at the bifurcation of the index-side carotid artery and perpendicular to the longitudinal direction of index-side carotid artery. The index-side was the symptomatic side if there was only one symptomatic side, otherwise, the left side. The SNAP images were acquired coronally along the artery. The traditional multi-contrast acquisition covered about 48 mm of carotid artery in head-feet direction with about 12 min scan, and the 3D SNAP acquisition covered the whole carotid artery and part of intracranial arteries (250 mm in head-feet direction) with about 7 min scan. The scan parameters were summarized in Table 1. The study protocol was approved by the Institution Review Board of Tsinghua University School of Medicine prior to the initiation of this study and the written informed consent was obtained from each subject before participating the original study.

Table 1
The scan parameters for the traditional multi-contrast sequences (T1W, T2W, and TOF) and SNAP.

	T1W	T2W	TOF	SNAP
Sequence	T1W-QIR	T2W-DIR	3D TOF	3D SNAP
TE (ms)	10	50	5	5
TR (ms)	800	4800	20	10
Matrix size	268 × 260	268 × 260	268 × 267	312 × 312
Number of slices	16	16	48	100
Slice thickness (mm)	2	2	1	0.8
In-plane FOV (mm^2)	160 × 160	160 × 160	160 × 160	250 × 250
In-plane resolution (mm^2)	0.6 × 0.6	0.6 × 0.6	0.6 × 0.6	0.8 × 0.8
Acquisition plane	Axial	Axial	Axial	Coronal
Scan time	6min 11s	3min 50s	2min 4s	7min 1s

2.2. Multiple contrast SNAP images generation

In SNAP sequence, the inversion recovery (IR) and reference (REF) images were directly acquired from two successive gradient echo acquisitions [13]. After the phase-sensitive reconstruction (CR) image was generated [13], the SNAP2 image [14] was then derived as: $IR \cdot REF^* / \|IR\|$, where $*$ represented complex conjugation. Thus, one SNAP acquisition can generate four images, including IR, REF, CR and SNAP2. Notably, all these images were inherently co-registered because they were generated from one acquisition. Six image sets, including the magnitude, the real part and imaginary part of the IR, the magnitude of REF and CR and the real part of SNAP2 were used as the intensity features of each pixel for further analysis, and the exemplary images were shown in Fig. 1.

2.3. SNAP training set

The pre-processing procedures to generate the ground truth of SNAP training set were shown in Fig. 2. Firstly (Step 1 in Fig. 2), on the traditional multi-contrast images, the boundaries of lumen and the outer wall were manually delineated, and the calcification (CA), lipid-rich/necrotic core (LRNC) and intraplaque hemorrhage (IPH) were manually delineated by two radiologists with consensus agreement based on an established review criteria [8] using a custom-designed software (CASCADE [21]). Notably, IPH was identified to be part of LRNC, as previous studies [6,22–25]. The two radiologists (B.S. and X.Z.) had > 5 years' experience in vascular imaging. The rest part of the vessel wall (the region inside the contour of outer wall and outside the contour of the lumen) was considered as the fibrous tissue (FT). Secondly (Step 2 in Fig. 2), the original SNAP images were resliced according to the thickness and spatial location of the traditional multi-contrast images. Thirdly (Step 3 in Fig. 2), for each artery, the manually delineated component contours from the multi-contrast images were mapped to the resliced SNAP images allowing manual adjustment. The contour mapping was done by another reviewer (H.Q.) blinded to patient information. The traditional multi-contrast images were scored using an established four-level criteria [26]. The resliced SNAP image

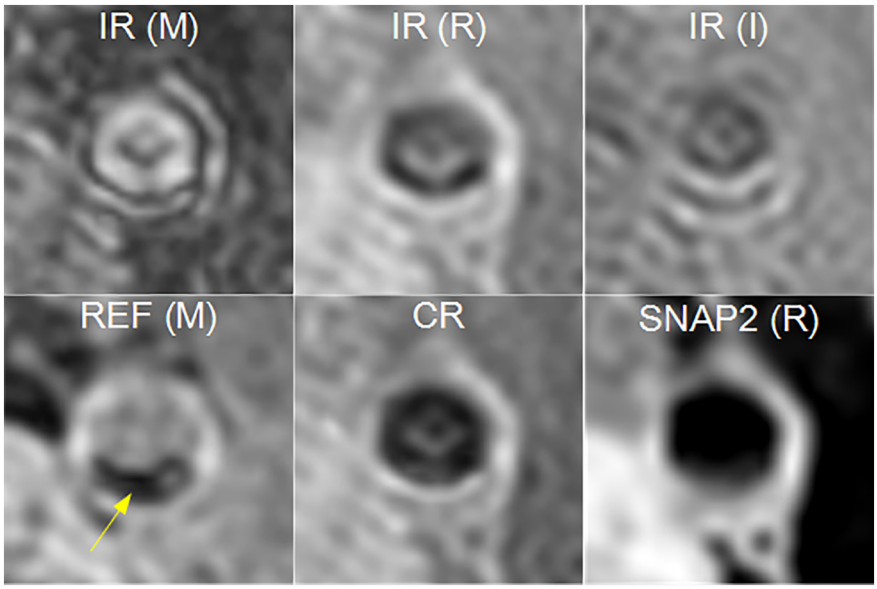

Fig. 1. Multiple contrast images derived from a single SNAP acquisition of the left carotid artery of a patient (male, 51 years old) with calcification (the yellow arrow), including the inversion recovery acquisition (IR), reference acquisition (REF), phase-sensitive reconstruction (CR), SNAP2 image. In the bracket, M indicated magnitude, R indicated real, I indicated imaginary. (For interpretation of the references to colour in this figure legend, the reader is referred to the web version of this article.)

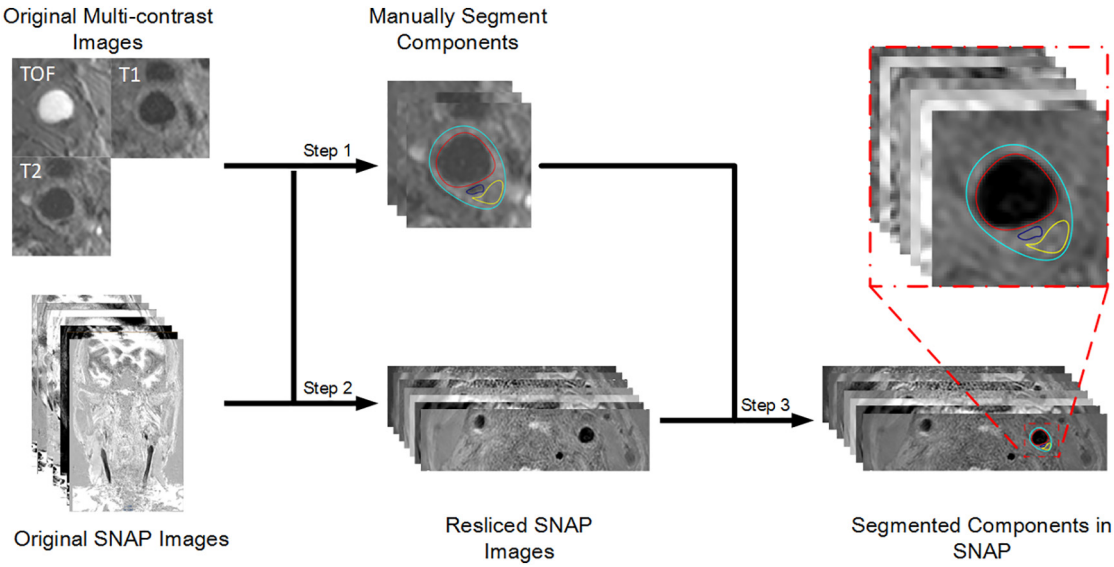

Fig. 2. The process of generating the SNAP training set. 1) Step1: Manually segment components in traditional multi-contrast images using an established review protocol [8]; 2) Step 2: Resliced SNAP images according to the thickness and spatial location of the traditional multi-contrast images; 3) Step 3: Map the manually segmented contours from the multi-contrast images to the resliced SNAP images.

was scored as good image quality if the CR image showed good lumen delineation in which less than half of the lumen boundary was obscure or invisible, otherwise the image was scored as poor quality. The registration quality of mapping the contour was scored as good/poor according to whether the contours could match the resliced SNAP image. The slices with poor image quality for both traditional multi-contrast and the resliced SNAP images were excluded from this study, and the resliced SNAP images with poor registration to the traditional multi-contrast images due to patient motion were excluded from the analysis. In this way, each pixel on the resliced SNAP images can be labeled as CA, IPH, LRNC or FT. All the images were interpolated to an in-plane spatial resolution of $0.31 \times 0.31\ mm^2$.

2.4. Feature calculation and pre-processing

For each pixel of the vessel wall, intensity and morphological features were calculated. For the intensity features, each SNAP image was divided by its median signal intensity within the 4 cm diameter circular ROI centering at the carotid artery to normalize the absolute intensity of each pixel [12,27]. There were six intensity features, including the real/imaginary/magnitude part of IR, the magnitude part of REF and CR and the real part of SNAP2. As for the morphological features, the Delaunay triangulation algorithm [28] was used to determine the local thickness of the vessel wall and the distance from the pixel to lumen [12].

Notably, the CR and SNAP2, which can be used to detect the plaque components by experienced reviewers [13,14], can be calculated from the imaginary/real part of IR and REF. However, it was unclear whether the machine learning methods can automatically utilize this information. Thus, this study also tested the performance of classifiers using morphological features plus all six intensity features, four intensity features (imaginary/real part of IR and REF), and two intensity features (CR and SNAP2).

Table 2
Information of slices.

Variable	Number. (%) or Mean ± SD
Stenosis (%)	11.9 ± 25.5
Number of image slices of AHA type (N = 1436)	
Type I-II	814 (56.7%)
Type III	214 (14.9%)
Type IV-V	299 (20.8%)
Type VI	34 (2.4%)
Type VII	72 (5.0%)
Type VIII	3 (0.2%)
Number of image slices containing different plaque components (N = 1436)	
IPH	37 (2.6%)
CA	156 (10.9%)
LRNC	331 (23.1%)
Number of arteries containing different plaque components (N = 136)	
IPH	10 (7.4%)
CA	49 (36.0%)
LRNC	90 (66.2%)

AHA: American Heart Association [8], IPH: intraplaque hemorrhage, CA: calcification, LRNC: lipid-rich/necrotic core.

2.5. Machine learning methods

The training of machine learning classifiers consisted of two steps. Firstly, LRNC (with or without IPH), CA and FT were identified for all images, and then the IPH was segmented from LRNC. Resampling was carried out before the training, because the imbalanced sample sizes of the training data may affect the performance of the machine learning methods. In the first step, the CA was up-sampled to the data size of LRNC, and the FT was down-sampled to the sum of CA and LRNC. In the second step, the IPH was up-sampled to the data size of LRNC. All the up-sampling was done by using MOTE algorithm [29], and all the down-sampling was done by randomly selecting pixels from the original data.

Five classifiers were compared for segmentation of plaque components, including Naive Bayes (NB) [30], Support Vector Machine (SVM) [31], Random Forest (RF) [32], Gradient Boosting Decision Tree (GBDT) [33], and Artificial Neural Network (ANN) [34]. The input was the features extracted in Section 2.4, the output was the probability that the pixel belong to each component, and the parameters used in the classifiers were shown in the Supporting Information.

2.6. Contour generation

Once the probabilities for each pixel were calculated by the classifiers, the final step was to classify each pixel as a given component. We utilized the level set method [35] on the probability map generated from the machine learning classifiers to define the final contours of CA, IPH and LRNC. This step of contour generation was necessary considering its two benefits: 1) it helps to eliminate isolated pixels and convoluted regions caused by noise; 2) the contour generation procedure provides the flexibility for users to manually adjust the segmentation if necessary.

2.7. Evaluation

In this study, the artery-wise and slice-wise 10-fold cross validations were used to test the segmentation performance for the first step and second step, respectively. All arteries were partitioned into 10 subsamples for the first step, and the slices containing LRNC were partitioned into 10 subsamples for the second step, then the pixels of nine subsamples of data were used as the training data. For the remaining data, all pixels were used as the test data for the first step, and the pixels which were predicted as LRNC in the first step were used as the test data for the second step.

The overall pixel-wise accuracy of each classifier in the test was reported. The Pearson's correlation coefficients of the areas of plaque components between the manual and the proposed segmentation were calculated since the area was the fundamental marker in plaque components quantification [36,37]. Then, the sensitivities & specificities and Youden's indexes [38] of presence of LRNC and CA in all slices (first step) and of IPH for the slices containing LRNC (second step) were evaluated because the presence of components was an important indicator for plaque stability [2,39,40].

3. Results

There were 177 slices with poor traditional multi-contrast quality and 277 slices with poor resliced SNAP quality because of the motion artifact and flow artifact, and 227 slices with poor registration quality between the resliced SNAP and traditional multi-contrast image. After excluding those slices, 1436 slices of carotid artery were included for further analysis. The details of these slices were shown in Table 2, including stenosis, American Heart Association (AHA) type [8] and number of plaques. Finally, the number of pixels was 7435 for CA, 25365 for LRNC and 443,146 for FT, and there were 2298 pixels of IPH among LRNC.

In the first step that segmented LRNC (with or without IPH), CA and FT, the quantified LRNC, CA and FT areas of all the tested classifiers were significantly correlated with manual segmentations (Table 3). Correlation coefficients of RF, GBDT, and ANN using six intensity features were higher than using fewer intensity features, and the correlation coefficients were all higher than 0.80 for LRNC and 0.79 for CA. The overall pixel-wise accuracy using six intensity features was: 0.91 (NB), 0.90 (SVM), 0.91 (RF), 0.89 (GBDT) and 0.89 (ANN). Table 4 showed the sensitivity & specificity and Youden's index to detect LRNC and CA for all analyzed slices. The Youden's indexes of RF, GBDT and ANN were all higher than 0.79 for LRNC and 0.76 for CA, and were better than NB and SVM.

In the second step that segmented IPH from LRNC, the overall pixel-wise accuracy of classification for each method was: 0.78 (NB), 0.88 (SVM), 0.80 (RF), 0.82 (GBDT) and 0.84 (ANN). The quantified IPH areas of all the tested classifiers were significantly correlated with manual segmentation (Table 5). The correlation coefficients of RF, GBDT and ANN were all higher than 0.62. On the other hand, the NB and SVM classifiers had relative low correlation coefficients. Table 5 also showed the sensitivity & specificity and Youden's index, and the RF classifier achieved the highest Youden's index (0.69).

Table 3
Correlation coefficients of areas of LRNC (with or without IPH), CA and FT using morphological and three kinds of intensity features: all six intensity features, four intensity features (imaginary/real part of IR and REF) and two intensity features (CR and SNAP2).

	NB	SVM	RF	GBDT	ANN
LRNC (***)	0.73/0.72/0.76	0.64/0.70/0.71	0.83/0.81/0.79	0.82/0.80/0.79	0.83/0.78/0.76
CA (***)	0.71/0.66/0.65	0.78/0.69/0.63	0.80/0.72/0.65	0.79/0.73/0.65	0.80/0.72/0.62
FT (***)	0.89/0.93/0.90	0.88/0.90/0.86	0.89/0.87/0.85	0.84/0.84/0.85	0.83/0.82/0.84

IR: inversion recovery acquisition, REF: reference acquisition, CR: phase sensitive reconstruction, ***: $p < 0.001$ for three kinds of intensity features and five classifiers, LRNC: lipid-rich/necrotic core, CA: calcification, FT: fibrous tissue, NB: Naive Bayes, SVM: Support Vector Machine, RF: Random Forest, GBDT: Gradient Boosting Decision Tree, ANN: Artificial Neural Network.

Table 4
Sensitivities & specificities and Youden's indexes of presence of LRNC (with or without IPH) and CA for all analyzed slices.

	NB	SVM	RF	GBDT	ANN
LRNC	0.83/0.88/0.70	0.83/0.86/0.69	0.91/0.89/0.79	0.95/0.85/0.80	0.95/0.85/0.80
CA	0.68/0.93/0.61	0.73/0.92/0.65	0.83/0.93/0.77	0.86/0.91/0.77	0.90/0.88/0.77

LRNC: lipid-rich/necrotic core, CA: calcification, NB: Naive Bayes, SVM: Support Vector Machine, RF: Random Forest, GBDT: Gradient Boosting Decision Tree, ANN: Artificial Neural Network.

Table 5
The correlation coefficients of the areas of IPH between manual and proposed segmentation and sensitivity & specificity & Youden's index of presence of IPH.

	NB	SVM	RF	GBDT	ANN
Correlation coefficient	0.45 ($p < 0.001$)	0.58 ($p < 0.001$)	0.63 ($p < 0.001$)	0.62 ($p < 0.001$)	0.63 ($p < 0.001$)
Sensitivity	0.35	0.46	0.81	0.78	0.70
Specificity	0.93	0.95	0.87	0.86	0.87
Youden's index	0.28	0.41	0.69	0.65	0.57

IPH: intraplaque hemorrhage, NB: Naive Bayes, SVM: Support Vector Machine, RF: Random Forest, GBDT: Gradient Boosting Decision Tree, ANN: Artificial Neural Network.

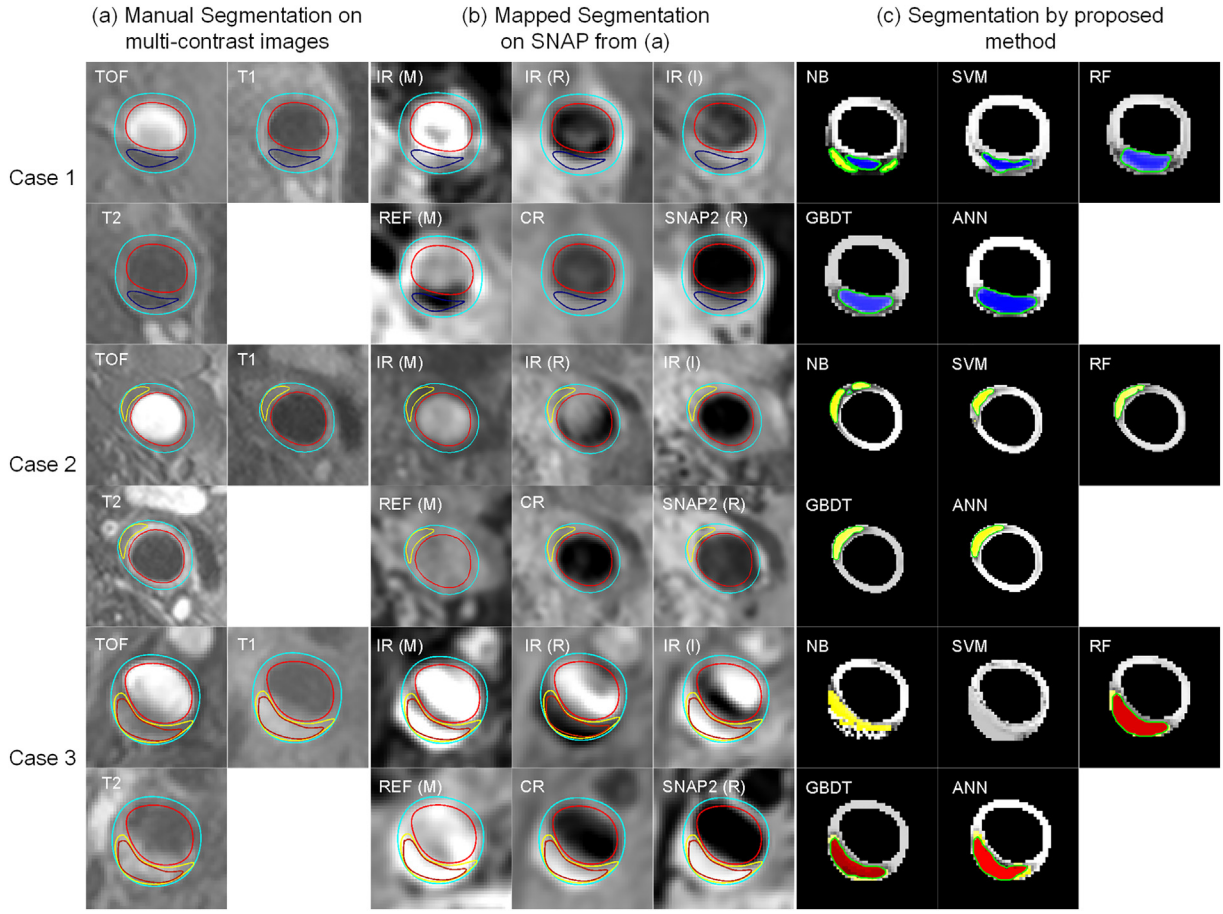

Fig. 3. The example cases (rows) of segmentation for CA (Case 1) and LRNC (Case 2) in the first step and IPH (Case 3) in the second step. (a, b) manual segmentation on multi-contrast images and mapped segmentation on SNAP images. The contours indicated lumen (red), outer wall (cyan), CA (blue), IPH (dark red) and LRNC (yellow); (c) the probability map and region contours generated from five classifiers: Naive Bayes (NB), Support Vector Machine (SVM), Random Forest (RF), Gradient Boosting Decision Tree (GBDT), and Artificial Neural Network (ANN). The colors indicate the component with the highest probability: CA in blue, IPH in red, LRNC in yellow and FT in gray, while the intensity represented the probability that the pixel being the component. The green contours indicated the final segmentation after contour generation. (For interpretation of the references to colour in this figure legend, the reader is referred to the web version of this article.)

Fig. 3 showed the examples of segmentations of five classifiers for the first step (Case 1–3) and the second step (Case 3). In the segmentation of CA and LRNC (without IPH), the RF, GBDT and ANN all generated similar results as manual segmentations (Fig. 3, Case 1 & 2). In the segmentation of LRNC with IPH (Fig. 3, Case 3), the SVM failed to segment LRNC and NB segment less LRNC, while RF, GBDT and ANN yielded similar segmentations as manual results. In the segmentation of IPH from LRNC in the second step (Fig. 3, Case 3), the NB failed to segment IPH from LRNC, and the segmented IPH of RF & GBDT was more similar with manual segmentation than that of ANN.

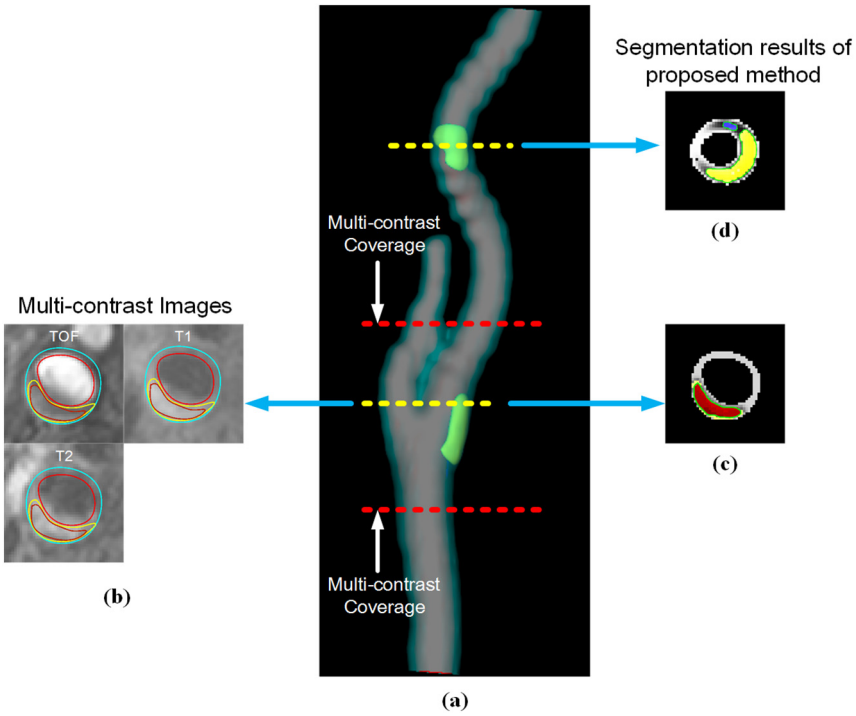

Fig. 4. One example of segmentation results from the 3D SNAP data using our proposed two steps method. (a) The surface rendering of lumen (red), outer wall (cyan), CA (blue), LRNC (yellow) of an example artery. The red dotted lines indicate the coverage of traditional multi-contrast images. The yellow dotted lines indicate one cross-sectional plane inside the coverage of traditional multi-contrast images (b, c) and one cross-sectional plane imaged by SNAP but not imaged by traditional multi-contrast images (d). (b) The manual segmentation on traditional multi-contrast images, the contours indicated lumen (red), outer wall (cyan), IPH (dark red) and LRNC (yellow). (c) The segmentation result of the same slice in (b) using proposed method. (d) The proposed method with GBDT successfully segment a slice with CA and LRNC outside the coverage of traditional multi-contrast images. The colour in (c) and (d) indicate the component with the highest probability CA in blue, IPH in red, LRNC in yellow and FT in gray, while the intensity represents the probability that the pixel was classified to the component. (For interpretation of the references to colour in this figure legend, the reader is referred to the web version of this article.)

Notably, the coronal SNAP image has a much larger coverage than the traditional multi-contrast images. As the example shown in Fig. 4, the proposed two steps method with GBDT classifier can successfully segment not only the plaque components as the traditional multi-contrast images, but also the plaque components beyond the coverage of traditional multi-contrast images.

4. Discussion

This study proposed a segmentation method for plaque components using a single SNAP sequence. Different from previous studies to identify intraplaque hemorrhage [13] and calcification [16] manually, this study validates the feasibility of automatic plaque components segmentation methods by using a two steps machine learning method. Furthermore, by utilizing both the intensity and morphological features, this study showed that machine learning method has the ability to identify LRNC in carotid plaques on SNAP images. Traditionally, LRNC was identified on contrast-enhanced double inversion recovery T1 weighted images [41] or T2 weighted images [42]. A recent study [17] found that LRNC can be identified on a heavily T1 weighted sequence (MPRAGE), on which the small T1 difference between LRNC and FT [43] may be more obvious than on traditional double inversion recovery T1 weighted images. The SNAP sequence used in this study is also a heavily T1 weighted sequence, which may also provide similar intensity difference to facilitate LRNC identification. In addition, morphological features have been proven to be helpful in segmentation of LRNC and other plaque components [12]. Furthermore, machine learning method should be more effective than manual segmentation to distinguish slight signal difference and integrate intensity and morphological information together. These factors may explain the results that LRNC can be detected by using machine learning method on SNAP images.

Thus, with outlined lumen and outer wall boundary, the proposed segmentation method by using SNAP sequence can be used to identify important plaque features including IPH, LRNC and CA. Moreover, the different contrast images calculated from SNAP were inherently co-registered. Thus, possible misregistration among traditional multi-contrast images, which was caused by non-rigid motion in carotid, can be avoided. Furthermore, compared with traditional multi-contrast protocol, the SNAP is a 3D sequence with much larger coverage (48 mm vs. 250 mm) and shorter scan time (12 min vs. 7 min). As shown in Fig. 4, the proposed two steps segmentation method using SNAP can quantify plaque components of carotid artery in a much larger coverage. Thus, the proposed segmentation method using one single SNAP may be a promising tool for carotid atherosclerotic plaque assessment.

This study tested different combinations of intensity features generated from SNAP sequence in the first step to segment LRNC (with or without IPH), CA and FT. The results showed that using all the six intensity features could benefit the plaque components segmentation performance other than using four or two intensity features (Table 3), although some intensity features can be calculated from other intensity features. We believed that the reason was that the limited sample size of training data used in this study was not enough to train the classifiers from the four/two intensity features. Furthermore, this study also tested five different classifiers in plaque components segmentation. The RF, GBDT and ANN all showed similar high correlation coefficients and Youden's indexes in segmenting LRNC (with or without IPH) and CA in the first step, but RF classifier showed the highest Youden's index in the second step to segment IPH from LRNC. Although the overall pixel-wise accuracy is not very low in the first and second step, the NB and SVM classifiers showed lower correlation coefficients and the Youden's indexes than the other three classifiers. Thus, we believed that the RF classifiers was the overall best classifier for plaque components segmentation in our proposed two steps method.

In the population of this study, the prevalence of IPH was relative low compared with previous studies [2,44,45]. The reason may be that the stenosis degree of the patients included in this study was not as high as those studies since a recent study [46] reported a much lower IPH presence in symptomatic arteries with mild stenosis than that with severe stenosis. Moreover, this study also included the asymptomatic arteries, which further lower the prevalence of IPH. The limited sample size of IPH poses a challenge to accurately segment IPH for machine learning methods. Thus, we utilized a two steps segmentation method and sample size adjusting method to overcome this challenge. Although the performance of the second step to identify IPH from LRNC is not as good as the first step, the feasibility to do so was validated. Thus, future

studies with larger sample size are still needed to further validate the proposed method.

This study also suffered from some limitations. First, this study used the manual segmentation of plaque components on non-contrast multi-weighting MR images as the reference because the data used in this retrospective study did not include contrast enhanced MRI. Although this non-contrast multi-weighting MR protocol have been validated with histology [8,42,47] in identify plaque components, histological ground truth should be included in future studies to further validate the proposed method. Second, the predefined lumen and outer wall were still needed, and the contours transferring from traditional protocol to SNAP image may introduce some bias to the segmentation result because of the mis-registration between the SNAP and multi-contrast images caused by patient motion. Deep learning method could be further investigated to automatically segment lumen and outer wall in SNAP images [48]. Third, the low presence of fibrotic plaque (type VIII, 0.2%) made it difficult to validate the performance of our proposed method to images containing type VIII plaque. Larger populations with enough type VIII plaque are needed in future studies. Lastly, the relative long scan time (7 min) and low spatial resolution of SNAP sequence effect the segmentation results. Fast imaging methods, such as Goal-SNAP [49] or fSNAP [50] could be used to further improve the our proposed method.

5. Conclusions

The feasibility of using SNAP to identify plaque components, including LRNC, IPH, CA and FT has been validated by using the proposed method. Thus, the proposed segmentation method using a single SNAP might be a promising tool for atherosclerotic plaque components assessment.

Acknowledgements and disclaimer

This work was supported by grants of National Natural Science Foundation of China (81371540, 81571667, 81771825 and 81271536). The study protocol was approved by the local Institution Review Board. Information presented is based on research and is not commercially available.

Appendix A. Supplementary data

Supplementary data to this article can be found online at https://doi.org/10.1016/j.mri.2019.04.001.

References

[1] Organization, W.H. Cardiovascular diseases (CVDs). 2016.
[2] Hosseini AA, Kandiyil N, Macsweeney STS, Altaf N, Auer DP. Carotid plaque hemorrhage on magnetic resonance imaging strongly predicts recurrent ischemia and stroke. Ann Neurol 2013;73(6):774–84.
[3] Redgrave JN, Lovett JK, Gallagher PJ, Rothwell PM. Histological assessment of 526 symptomatic carotid plaques in relation to the nature and timing of ischemic symptoms: the Oxford plaque study. Circulation 2006;113(19):2320–8.
[4] Wahlgren CM, Zheng W, Shaalan W, Tang J, Bassiouny HS. Human carotid plaque calcification and vulnerability. Cerebrovasc Dis 2009;27(2):193–200.
[5] Virmani R, Ladich ER, Burke AP, Kolodgie FD. Histopathology of carotid atherosclerotic disease. Neurosurgery 2006;59(5 Suppl 3):S219–27. [discussion S3-13].
[6] Saam T, Ferguson MS, Yarnykh VL, Takaya N, Xu D, et al. Quantitative evaluation of carotid plaque composition by in vivo MRI. Arterioscler Thromb Vasc Biol 2005;25(1):234–9.
[7] Zhao X, Underhill HR, Yuan C, Oikawa M, Dong L, et al. Minimization of MR contrast weightings for the comprehensive evaluation of carotid atherosclerotic disease. Invest Radiol 2010;45(1):36–41.
[8] Cai J-M, Hatsukami TS, Ferguson MS, Small R, Polissar NL, et al. Classification of human carotid atherosclerotic lesions with in vivo multicontrast magnetic resonance imaging. Circulation 2002;106(11):1368–73.
[9] Clarke SE, Hammond RR, Mitchell JR, Rutt BK. Quantitative assessment of carotid plaque composition using multicontrast MRI and registered histology. Magn Reson Med 2003;50(6):1199–208.
[10] te Boekhorst BC, van 't Klooster R, Bovens SM, van de Kolk KW, Cramer MJ, et al. Evaluation of multicontrast MRI including fat suppression and inversion recovery spin echo for identification of intra-plaque hemorrhage and lipid core in human carotid plaque using the mahalanobis distance measure. Magn Reson Med 2012;67(6):1764–75.
[11] Adame IM, van der Geest RJ, Wasserman BA, Mohamed MA, Reiber JH, et al. Automatic segmentation and plaque characterization in atherosclerotic carotid artery MR images. MAGMA 2004;16(5):227–34.
[12] Liu F, Xu D, Ferguson MS, Chu B, Saam T, et al. Automated in vivo segmentation of carotid plaque MRI with morphology-enhanced probability maps. Magn Reson Med 2006;55(3):659–68.
[13] Wang J, Börnert P, Zhao H, Hippe DS, Zhao X, et al. Simultaneous non-contrast angiography and intraPlaque hemorrhage (SNAP) imaging for carotid atherosclerotic disease evaluation. Magn. Reson. Med. 2013;69(2):337–45.
[14] Balu N, Sun J, Hippe DS, Chen H, Yuan C. Measurement of plaque burden using 3D SNAP vessel wall MRI. International Society for Magnetic Resonance in medicine. 2016. [Singapore].
[15] Chen, S., H. Zhao, J. Li, Z. Zhou, R. Li, et al., Evaluation of carotid atherosclerotic plaque surface characteristics utilizing simultaneous noncontrast angiography and intraplaque hemorrhage (SNAP) technique. J Magn Reson Imaging.
[16] Balu N, Sun J, Liu J, Chen S, Chen H, et al. Assessment of calcification size and juxtaluminal status using gray-blood 3D vessel wall MRI. International society for magnetic resonance in medicine. 2015. [Tornto, Ontario, Canada].
[17] Qiao H, Li F, Xu D, Liu G, Yuan C, et al. Identification of carotid lipid-rich necrotic core and calcification by 3D magnetization-prepared rapid acquisition gradient-echo imaging. Magn Reson Imaging 2018;53:71–6.
[18] Zhou Z, Li R, Zhao X, He L, Wang X, et al. Evaluation of 3D multi-contrast joint intra- and extracranial vessel wall cardiovascular magnetic resonance. J Cardiovasc Magn Reson 2015;17:41. https://doi.org/10.1186/s12968-015-0143-z.
[19] Yarnykh VL, Yuan C. T1-insensitive flow suppression using quadruple inversion-recovery. Magn Reson Med 2002;48(5):899–905.
[20] Yarnykh VL, Yuan C. Multislice double inversion-recovery black-blood imaging with simultaneous slice reinversion. J Magn Reson Imaging 2003;17(4):478–83.
[21] Kerwin W, Xu D, Liu F, Saam T, Underhill H, et al. Magnetic resonance imaging of carotid atherosclerosis: plaque analysis. Top Magn Reson Imaging 2007;18(5):371–8.
[22] Chun, Y., K.W. S., Y.V. L., C. Jianming, S. Tobias, et al., MRI of atherosclerosis in clinical trials. NMR Biomed, 2006. 19(6): p. 636–654.
[23] Yuan C, Mitsumori LM, Ferguson MS, Polissar NL, Echelard D, et al. In vivo accuracy of multispectral magnetic resonance imaging for identifying lipid-rich necrotic cores and Intraplaque hemorrhage in advanced human carotid plaques. Circulation 2001;104(17):2051–6.
[24] Yoshida K, Narumi O, Chin M, Inoue K, Tabuchi T, et al. Characterization of carotid atherosclerosis and detection of soft plaque with use of black-blood MR imaging. Am J Neuroradiol 2008;29(5):868–74.
[25] Mono ML, Karameshev A, Slotboom J, Remonda L, Galimanis A, et al. Plaque characteristics of asymptomatic carotid stenosis and risk of stroke. Cerebrovasc Dis 2012;34(5–6):343–50.
[26] Zhou Z, Li R, Zhao X, He L, Wang X, et al. Evaluation of 3D multi-contrast joint intra- and extracranial vessel wall cardiovascular magnetic resonance. J Cardiovasc Magn Reson 2015;17(1):41.
[27] Liu J, Balu N, Hippe DS, Ferguson MS, Martinez-Malo V, et al. Semi-automatic carotid intraplaque hemorrhage detection and quantification on magnetization-prepared rapid acquisition gradient-Echo (MP-RAGE) with optimized threshold selection. J Cardiovasc Magn Reson 2016;18:41.
[28] Yuan C, Han C. Plaque morphological quantitation. Angiography and plaque imaging. CRC Press; 2003. p. 365–96.
[29] Chawla NV, Bowyer KW, Hall LO, Kegelmeyer WP. SMOTE: synthetic minority over-sampling technique. J. Artif. Intell. Res. 2002;16(1):321–57.
[30] Zhang H. The optimality of naive Bayes. vol. 2. 2004.
[31] Boser BE, Guyon IM, Vapnik VN. A training algorithm for optimal margin classifiers. Proceedings of the fifth annual workshop on computational learning theory. Pittsburgh, Pennsylvania, USA: ACM; 1992. p. 144–52.
[32] Breiman L. Random Forests. Mach Learn 2001;45(1):5–32.
[33] Friedman JH. Greedy function approximation: a gradient boosting machine. Ann Statist 2001;29(5):1189–232.
[34] Li J, Cheng J-h, Shi J-y, Huang F. Brief introduction of back propagation (BP) neural network algorithm and its improvement. In: Jin D, Lin S, editors. Advances in computer science and information engineering. Vol. 2. Berlin, Heidelberg: Springer Berlin Heidelberg; 2012. p. 553–8.
[35] Chunming L, Chenyang X, Changfeng G, Fox MD. Level set evolution without re-initialization: A new variational formulation. 2005 IEEE computer society conference on computer vision and pattern recognition (CVPR'05). 2005.
[36] de Weert TT, Ouhlous M, Meijering E, Zondervan PE, Hendriks JM, et al. In vivo characterization and quantification of atherosclerotic carotid plaque components with multidetector computed tomography and histopathological correlation. Arterioscler Thromb Vasc Biol 2006;26(10):2366–72.
[37] Touzé E, Toussaint J-F, Coste J, Schmitt E, Bonneville F, et al. Reproducibility of high-resolution MRI for the identification and the quantification of carotid atherosclerotic plaque components. Consequences for prognosis studies and therapeutic trials. **vol. 38(6)**. 2007. p. 1812–9.
[38] J. YW. Index for rating diagnostic tests. Cancer 1950;3(1):32–5.
[39] Redgrave JNE, Lovett JK, Gallagher PJ, Rothwell PM. Histological assessment of 526 symptomatic carotid plaques in relation to the nature and timing of ischemic symptoms. Oxford Plaque Study 2006;113(19):2320–8.
[40] Virmani R, Ladich ER, Burke AP, Kolodgie FD. Histopathology of carotid atherosclerotic disease. Neurosurgery 2006;59(5). [p. S3-219-S3-227].

[41] Cai J, Hatsukami TS, Ferguson MS, Kerwin WS, Saam T, et al. In vivo quantitative measurement of intact fibrous cap and lipid-rich necrotic core size in atherosclerotic carotid plaque. Comparison of High-resolution, Contrast-enhanced Magnetic Resonance Imaging and Histology. 112(22). 2005. p. 3437–44.
[42] Trivedi RA, U-King-Im J-M, Graves MJ, Horsley J, Goddard M, et al. MRI-derived measurements of fibrous-cap and lipid-core thickness: the potential for identifying vulnerable carotid plaques in vivo. Neuroradiology 2004;46(9):738–43.
[43] Jiang Y, Zhu C, Peng W, Degnan AJ, Chen L, et al. Ex-vivo imaging and plaque type classification of intracranial atherosclerotic plaque using high resolution MRI. Atherosclerosis 2016;249:10–6.
[44] Altaf N, MacSweeney Shane T, Gladman J, Auer Dorothee P. Carotid intraplaque hemorrhage predicts recurrent symptoms in patients with high-grade carotid stenosis. Stroke 2007;38(5):1633–5.
[45] Altaf N, Daniels L, Morgan PS, Auer D, MacSweeney ST, et al. Detection of intraplaque hemorrhage by magnetic resonance imaging in symptomatic patients with mild to moderate carotid stenosis predicts recurrent neurological events. J Vasc Surg 2008;47(2):337–42.
[46] Zhao X, Hippe DS, Li R, Canton GM, Sui B, et al. Prevalence and characteristics of carotid artery high-risk atherosclerotic plaques in Chinese patients with cerebrovascular symptoms: a Chinese atherosclerosis risk evaluation II study. J Am Heart Assoc 2017;6(8):e005831.
[47] Trivedi RA, U-King-Im J, Graves MJ, Horsley J, Goddard M, et al. Multi-sequence in vivo MRI can quantify fibrous cap and lipid core components in human carotid atherosclerotic plaques. Eur J Vasc Endovasc Surg 2004;28(2):207–13.
[48] Lin M, Chiu B, Zhang Q, Qiao H, Dou J, et al. U-net: convolutional networks for carotid artery wall segmentation in simultaneous non-contrast angiography and intra-plaque hemorrhage (SNAP) imaging. Paris, France: ISMRM; 2018.
[49] Qi H, Sun J, Qiao H, Chen S, Zhou Z, et al. Carotid intraplaque hemorrhage imaging with quantitative vessel wall T1 mapping: technical development and initial experience. Radiology 2018;287(1):276–84.
[50] Chen S, Ning J, Zhao X, Wang J, Zhou Z, et al. Fast simultaneous noncontrast angiography and intraplaque hemorrhage (fSNAP) sequence for carotid artery imaging. Magn Reson Med 2017;77(2):753–8.